Adv Polym Sci (2016) 270: 193–220
DOI: 10.1007/12_2015_314

Published online: 6 May 2015

Nanocomposites and Self-Assembled Structures via Controlled Radical Polymerization

Christian Rossner and Philipp Vana

Abstract We report recent findings on the formation of nanocomposites and self-assembled hybrid nanoarchitectures, in which controlled radical polymerization plays a key role. Specifically, we address how macromolecular design via these controlled methods can be used to flexibly guide the formation of hybrid nanoarchitectures in a rational and predetermined fashion. To this end, the role of polymeric architecture in tuning polymer/inorganic nanocomposite structures is examined.

Keywords Nanoparticles · Phase separation · Polymeric architecture · Reversible-deactivation radical polymerization · Self-assembly

Contents

C. Rossner and P. Vana (✉)
Institut für Physikalische Chemie, Georg-August-Universität Göttingen, Tammannstrasse 6, 37077 Göttingen, Germany
e-mail: pvana@uni-goettingen.de

Abbreviations

AFM	Atomic force microscopy
AgNP	Silver nanoparticle
ATRP	Atom-transfer radical polymerization
AuNP	Gold nanoparticle
CPB	Concentrated polymer brush
DC	Daoud−Cotton
DEGEMA	Diethyleneglycol ethylmethacrylate
DEGMMA	Diethylenegylcol methylmethacrylate
DLS	Dynamic light scattering
DMAEMA	*N*,*N*-Diemthylaminoethyl methacrylate
DMF	*N*,*N*-Dimethylformamide
DMSO	Dimethylsulfoxide
GMA	Glycidyl methacrylate
HBP	Hyperbranched polymer
IONP	Iron oxide nanoparticle
LAMP	Lipoic acid 2-hydroxy-3-(methacryloyloxy)-propyl ester
LCST	Lower critical solution temperature
MPC	2-(Methacryloyloxy)ethyl phosphorylcholine
NMR	Nuclear magnetic resonance
NMRP	Nitroxide-mediated radical polymerization
NP	Nanoparticle
PDMAEMA	Poly(*N*,*N*-diemthylaminoethyl methacrylate)
PdNP	Palladium nanoparticle
PEG	Poly(ethylene glycol)
PEO	Poly(ethylene oxide)
PGMA	Poly(glycidyl methacrylate)
PMAA	Poly(methacrylic acid)
PMMA	Poly(methyl methacrylate)
PMPC	Poly(2-(methacryloyloxy)ethyl phosphorylcholine)
PN^{i}PAAM	Poly(*N*-isopropylacrylamide)
POEGMA	Poly(oligo(ethylene glycol) methacrylate)
PS	Polystyrene
PVP	Poly(vinylpyridine)
RAFT	Reversible addition−fragmentation chain transfer
RDRP	Reversible-deactivation radical polymerization
SAXS	Small-angle X-ray scattering
SDPB	Semidilute polymer brush
SEC	Size-exclusion chromatography
SI	Surface-initiated
SiNP	Silica nanoparticle
stat	Statistical
TEM	Transmission electron microscopy

THF	Tetrahydrofuran
TTC	Trithiocarbonate

1 Introduction

Inorganic nanoparticles (NPs) have been recognized as building units for the construction of materials that take advantage of the specific properties of NPs [1]. In order to obtain particles that are compatible for incorporation into such materials, it is necessary to shield their reactive surfaces with stabilizing ligands. To this end, functionalization of NPs with a polymer shell is an attractive way to introduce colloidal stability and at the same time modulate the properties of the resulting nanomaterial and equip it with stimuli-responsiveness [2–4]. The functionalization of particles with polymer can be undertaken by two different approaches: Using the so-called in-situ functionalization, it is possible to induce NP formation in the presence of polymers, which act as stabilizers for the growing particles. This strategy can, for example, be implemented using water-soluble reversible addition−fragmentation chain transfer (RAFT) polymers with dithiobenzoate termini, which can be reduced to thiol groups in the presence of a gold or silver salt precursor, leading to stable nanocomposites [5]. Alternatively, NPs can be functionalized ex-situ after their synthesis and work-up, either directly with polymers ("grafting-to") or with an initiator/chain transfer agent for surface-initiated (SI) polymerizations ("grafting-from"). The types of inorganic particles most often used in nanocomposites, and therefore considered in this chapter, are noble metal NPs, metal oxide NPs, and quantum dots. Metal NPs are particularly interesting because of their unique optical properties, which stem from surface plasmon resonance [6]. As a result of their chemical stability and facile surface modification, gold nanoparticles (AuNPs) are extensively studied representatives of this class. They are also particularly interesting in the realm of controlled radical polymerization, as RAFT polymers inherently contain anchor groups for gold surfaces. It has been shown that trithiocarbonate (TTC) and dithiobenzoate groups attach to gold [7]. Although a value of 36 kJ mol^{-1} has been determined for the free energy of adsorption of phenyldithioesters on a particular type of AuNP [8], another recent study [9] suggested that polymers with TTC and dithioester end groups can form even denser layers than thiol-terminated (the functional group most often encountered for the coating of gold surfaces) [10] polymers. Metal oxide NPs can also be readily conjugated with polymers via established anchor moieties [11], while the choice of anchor group might also influence the structure of the resulting nanocomposites [12]. Their incorporation into hybrid materials with polymers could lead to modulation of mechanical properties and also to cost reduction.

Controlled radical polymerizations (also called reversible-deactivation radical polymerization, RDRP, according to IUPAC recommendations) offer a unique way to modulate polymeric materials at the molecular level. By exploiting a dormant state of the propagating macroradical, the fraction of irreversibly terminated species

among the produced macromolecules can be reduced to a small number, which imparts "living" characteristics to the system and therefore enables the formation of complex macromolecular architectures, such as block copolymers and star polymers. Under typical conditions, the macromolecular species are rapidly switched between the dormant and active state, which leads to an equal distribution of growth probabilities for all chains and can result in narrow molecular weight distributions. It is thus possible to produce uniform polymers with defined molecular characteristics. These characteristics are defined by a large parameter space (monomer composition, degree of polymerization, degree of branching, distribution of special functional groups, etc.), which opens a huge operational window for macromolecular engineers to design polymers to meet specific requirements. In this chapter, we examine the literature of the past 10 years to evaluate if and how macromolecular design by means of controlled radical polymerization can be used to prepare polymer/inorganic nanocomposite materials with controlled architectures (location of NPs in polymer matrices, interparticle spatial relations, etc.) and properties.

2 Linear Homopolymers

We consider in this section the simplest case of homopolymers attached to a solid substrate with one end group. The polymer is thus composed of exactly one particular monomeric repeating unit; the average degree of polymerization of which can be controlled via living radical polymerization techniques. Hence, this type of polymer contains two sorts of information: (i) the functional group that is repeatedly expressed in the polymeric side chain or at the chain end remote from the NP surface, and (ii) the average size of one macromolecule. Both features influence the properties of composite materials of inorganic particles with polymers on their surfaces.

Homopolymers with distinct side chain functionalities can be obtained directly through homopolymerization or after post-polymerization modification of a polymer with reactive functional groups in its backbone, which can act as a platform for the preparation of a library of homopolymers with defined side chain moieties [13, 14]. The polymeric backbone can be chosen such that stable nanocomposites with NPs in the respective solvent can be obtained. Such stabilizing polymers can, for example, be applied in NP functionalization together with destabilizing molecules in varying molar ratios in order to control the aggregation of NPs in colloidal dispersion [15]. Regarding the chemistry in the polymer side chains, it is particularly interesting to study homopolymer brushes in cases where the monomeric repeating unit is capable of undergoing specific interactions that are rather weak individually, but significantly enhanced in the case of multivalent interactions [16]. As a result of such multivalent interactions, materials with fundamentally new properties are obtained when homopolymers bearing weakly interacting repeating units are assembled on a solid support. An illustrative example of this

principle is the so-called glyco-cluster effect, which is the reason why nanocomposites with glycopolymers have been investigated extensively in recent years.

RAFT polymerization is arguably tolerant to functional groups present in the monomer to be polymerized and also provides end groups that can be used as surface attachment points with or without additional post-polymerization modification. Therefore, monomers bearing unprotected glucosamine [17], glucoseamido and lactobioamido [18], mannose [19], or galactose [20] moieties can be polymerized in a RAFT process and their polymers grafted to NP surfaces. As an alternative to the direct polymerization of glycomonomers, the sugar moiety can be clicked to the polymeric backbone in a tandem polymerization [3+2]-cycloaddition reaction [21]. Nanocomposites of glycopolymers with AuNPs form complexes with lectins, which can lead to AuNP clustering and result in a plasmon band red shift [17, 19]. This recognition through complex formation may even be glycopolymer-specific [17, 20]. Complex formation with lectins can be further exploited in developing cancer theranostics [22]: RAFT homopolymers with glucosamine in their side chains can also be used to prepare nanocomposites with iron oxide nanoparticles (IONPs) of different shapes. The authors demonstrated that these nanohybrids attached to cell membranes of HeLa carcinoma cells expressing glucose transporters on their membranes. Also, the internalization of IONPs coated with glycopolymer was significantly increased compared with unmodified IONPs. Furthermore, cubic shaped IONPs showed a higher probability of cellular uptake than spindle-shaped particles in two different cell lines [22].

It should be noted, however, that substrate recognition through gold nanocomposites with a homopolymer layer is indeed a broad concept not limited to glycochemistry: Recognition can also lead to quantitative and cation-specific detection [23]. AuNPs covered with poly(methacrylic acid) (PMAA) were shown to aggregate upon exposure to Cr^{3+} cations. This led to a concentration-dependent shift of the localized surface plasmon resonance absorption band. After exposure to analyte solution, the sensor could be recovered by removal of Cr^{3+} using EDTA. When the recognition element implemented into the polymer brushes is self-complementary, nanohybrids with a tendency to form assembled network structures are formed [24]. This can be realized by decorating RAFT polymers with the ureidopyrimidone moiety at the α-chain end and grafting those polymers to AuNPs with a sulfur-containing ω-end. Therefore, the functionality that acts as recognition element does not need to be incorporated into the polymeric backbone, but can instead be located at the dangling end of the polymer brush that is remote from the particle surface, as the monomeric repeating units act as spacers.

RDRP techniques allow the preparation of macromolecules with predetermined degree of polymerization and narrow molar mass distribution. When such macromolecules are grafted onto the surface of NPs, it is interesting to investigate whether this size information can be used to organize inorganic particles in ordered assemblies. Following this idea and using surface-initiated atom-transfer radical polymerization (SI-ATRP), Fukuda and coworkers assembled nanocomposites of AuNPs [25] and SiNPs [26] with a poly(methyl methacrylate) (PMMA) shell in a

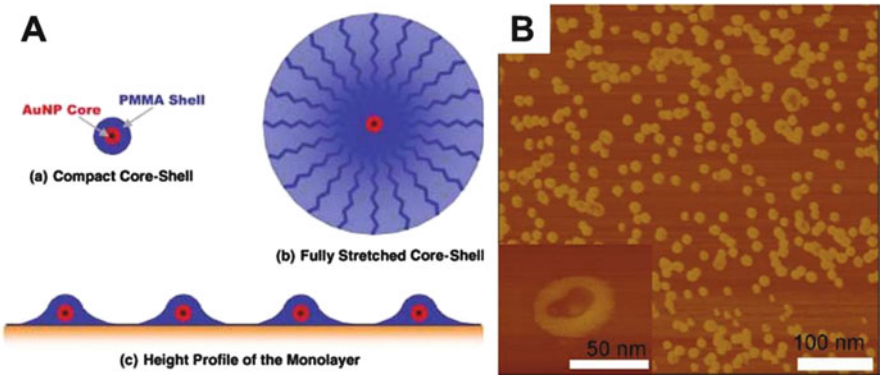

Fig. 1 (**a**) Structural model for a monolayer of hybrid particles, developed based on AFM measurements. Adapted with permission from [25]. Copyright 2003 Wiley-VCH Verlag GmbH & Co. KGaA, Weinheim. (**b**) Phase contrast AFM image showing a soft layer of polymer assembled around a hard gold particle core. Adapted with permission from [27]. Copyright 2009 American Chemical Society

two-dimensional array using Langmuir–Blodgett deposition. The authors found that the PMMA shell keeps the AuNP cores at certain distances, which increase with increasing graft chain length. Using atomic force microscopy (AFM), it was demonstrated that the PMMA forms a compact shell on top of AuNPs and a stretched shell around AuNPs, which causes the AuNP core spacings [25]. Analogous shell morphology in gold nanocomposites was also revealed by Davis and colleagues, who observed a soft shell assembled around a hard core in phase contrast AFM images of hybrid particles deposited on a solid substrate [27]. This indicates that the brushes on top of a particle were pulled downwards during the solvent evaporation process (Fig. 1).

When polymers are terminally grafted onto a surface at a high density, the surface-bound polymer adopts an extended conformation and stretches away from the surface; thus, the grafted polymer is in the concentrated polymer brush (CPB) regime. A unique feature of particle surfaces is that, as a result of their curvature, the concentration of polymer segments decreases in regions remote from the surface. This can lead to surface-bound polymer eventually going into the semidilute polymer brush (SDPB) regime, as a result of decreasing packing constraints [28, 29]. Dynamic light scattering (DLS) measurements of polymer brush height on individual nanohybrid particles [28, 30] and confocal laser scanning microscopy of three-dimensional colloidal crystals [28–31] confirm this behavior. The scaling of polymer brush height can be understood roughly in terms of a simple blob model pioneered by Daoud and Cotton [32]. This model was originally developed to describe star polymer conformations, but can also be applied to polymer brushes attached to a solid core. When the number of branches (i.e., the grafting density) is high, the individual branches adopt a stretched conformation in regions close to the core. Farther away from the core, the individual branches begin to relax because of the increased volume available for the chains, leading to a

different scaling of star radius with the number of repeat units in a branch N. For large N, the Daoud–Cotton (DC) model predicts a scaling of star radius (polymer brush height) of $\sim N^{0.6}$. This scaling is in agreement with polymer brush height measured by DLS in this regime [33]. However, the simple DC model fails to describe the behavior of brushes for smaller brush heights (i.e., when the chains are in the CPB regime). In this case, brush height was shown experimentally to scale with $\sim N^{0.8}$, an intermediate scaling between $\sim N^{0.6}$ and $\sim N^{1.0}$, the latter being the limit for highest grafting density and minimum surface curvature (i.e., dense polymer brushes on flat surfaces) [33]. Fukuda and coworkers applied the DC model to polymer brushes grafted onto a large core to investigate at what distance from the center of the particle the crossover from CPB to SDPB takes place [28]. This critical distance r_c was found to be given by:

$$r_c = r_o \times \sigma^{*1/2} \left((4\pi)^{1/2} \nu \right)^{-1}, \quad (1)$$

where r_o is the radius of the inorganic core, σ^* the dimensionless grafting density, and ν the excluded volume parameter. It follows that for small enough grafting densities, r_c is smaller than r_o and the whole polymer brush thus shows SDPB behavior. For large enough values of σ^* and small polymer brush heights, the entire brush shows CPB behavior. At a critical brush height, the CPB-to-SDPB transition occurs. Thus, the height of a polymer brush on an inorganic particle clearly scales with the degree of polymerization of the grafted chains, and the scaling behavior can provide information about whether the polymer is in the concentrated brush regime or not. This is valuable information, as it was recognized that the mechanical properties of self-assembled structures from hybrid particles are strongly influenced by the CPB–SDPB transition because more interparticle chain entanglements can occur in the SDPB case [34, 35]. The toughness of the hybrid materials of silica NPs with polystyrene (PS) and PMMA brushes was found to increase as the polymer brush height increased beyond the CPB–SDPB crossover [35]. On the other hand, material properties that do not depend much on polymer entanglements (i.e., the elastic modulus and hardness of the material) were shown to increase with increasing polymer brush molar mass and level off before the CPB–SDPB transition (Fig. 2) [35].

The state of the polymer brushes also affects the order formation in two-dimensional nanohybrid assemblies, because the SDPBs do not add significantly to the interparticle repulsive potential and act to dilute the array structure, resulting in decreased assembly order as the system goes far into the SDPB regime [36]. However, this behavior can be exploited intentionally by grafting bimodal polymer brushes, one of which is short and of high grafting density to shield the particle surface and one that is long with low grafting density, to achieve nanohybrids that can be more regularly dispersed in a polymer matrix [37], preventing particle assembly and structuring [38]. In such a molten state or blend, growing interparticle distances with increasing molecular weight of the surface-

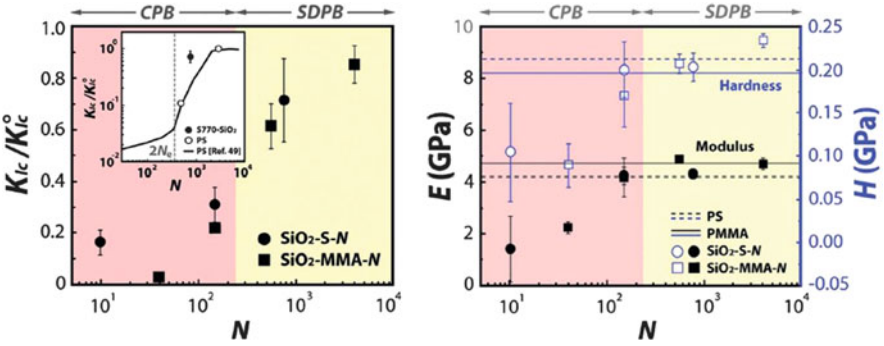

Fig. 2 Mechanical properties of nanocomposites of silica NPs with PS and PMMA. *Left*: Development of material toughness with increasing average number of monomeric repeat units per brush (N). *Right*: Dependence of elastic modulus E and hardness H on N. Adapted from [35] with permission of The Royal Society of Chemistry

bound polymer can also be observed by small-angle X-ray scattering (SAXS), and it was found that the interparticle distances can be further swollen by blending the hybrid particles with free polymer [39]. In the case of AuNPs, the gold core spacing results in unique optical responses, which stem from surface plasmon coupling [40] or, when the spacing is of the order of the wavelength of visible light, from Bragg diffraction [28, 31, 41].

Nanocomposites with a tailored polymer shell thickness can also be obtained through RAFT polymerization surface-initiated from silica [42, 43] and IONP surfaces [42], or via grafting-to approaches [44, 45]. The grafting-to strategy is particularly interesting because it can allow precise control of the polymer properties independently of the NP, prior to immobilization on a surface. For such an attachment of polymer chains, it is necessary that the enthalpy gain from the interaction of the anchor moiety with the surface balances the loss of entropy of the polymer chain. This entropy loss is reflected in a decrease in polymer grafting density with increasing average molecular weight of the employed polymer, which was verified for two types of AuNPs [45]. This behavior is logical, since the increased entropy loss (resulting from the conical confinement of longer polymer chains) can only be counterbalanced by more relaxed conformations as a result of their confinement in a larger space (i.e., by reducing the grafting density). When homopolymers are grafted to NPs with one end group, the question of whether they form brushes on the surface can be answered by determining the polymer shell thickness as a function of polymer molecular weight. This shell thickness can be quantified by systematically measuring the edge-to-edge distance between inorganic NP cores in self-assembled monolayers (Fig. 3) [44].

The data points obtained from the analysis of several TEM images can be fitted to a function describing the increase in interparticle distance with the increase in mean molar mass of grafted polymer. A simple yet suitable function can be chosen of the following form:

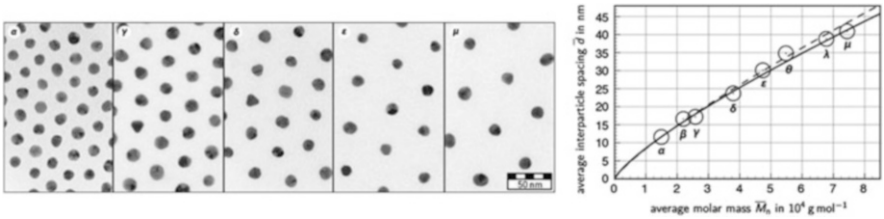

Fig. 3 *Left*: TEM images showing self-assembled monolayers from nanohybrid particles with gold cores and PN^{i}PAAM shells. The average degree of polymerization of N^{i}PAAM increases from *left* to *right*. *Right:* Dependence of interparticle spacing on the average degree of polymerization. Adapted with permission from [44]. Copyright 2013 American Chemical Society

$$\overline{d} = k \times \left[\overline{M}_n\right]^{1/l}. \tag{2}$$

A fit of (2) to the data yields $k = 6.02 \times 10^{-12}$ m and $1/l = 0.79$. When k is identified to be twice the contour length of the polymer and set fixed to this value (4.4×10^{-12} m), a value of 0.82 is obtained for the exponent $1/l$. Taking into consideration how the molar mass of surface-bound polymer translates to polymer shell thickness, this value obtained for $1/l$ might reflect densely grafted polymer brushes on the NP surface, provided that interparticle spacing in self-assembled monolayers can indeed be used as a measure of polymer shell thickness. That is, the information that is included in the scaling of interparticle distance with molar mass can be used to draw conclusions about the conformational state of the surface-anchored polymer chains.

3 Mixed Brushes of Two Different Linear Polymers

When two chemically different types of polymer are grafted to NPs, the situation becomes much more complex because the properties of both species influence the behavior of the resulting nanocomposites, depending on the individual chain lengths, grafting densities, and chemical properties of the two different brushes. Also, the different polymers might be grafted independently of each other, leading to a statistical distribution of both polymers on the surface, or they might be grafted as diblock copolymers at their block junction. Because the outcome of the latter results in mixed polymer brushes, we discuss this special case here and not in Sect. 3, which deals with copolymers in a more general sense. The behavior of nanocomposites with mixed brushes can reflect the properties of both polymeric species at the same time or it can be intermediate between those of NPs with uniform polymer brushes. Grafting of brushes with different solubility characteristics can lead to amphiphilic nanocomposites with a tendency to phase-separate on the surfaces. The phase separation of immobilized macromolecules into different domains is a unique feature of mixed brushes and is particularly interesting

because, unlike micelle formation in solutions containing free amphiphilic (macro) molecules, the outcome of the assembly is not influenced by the dilution of the system. Also, as shown in this section, phase separation in mixed brushes on NP surfaces and its modulation can prove useful in tuning nanocomposite properties and directing particle assembly.

Different surface morphologies (including rippled structures, different island structures with varying number of islands, and layered structures) resulting from microphase separation of two anchored polymer species can be predicted from a theoretical model, depending on the chain lengths and composition of mixed brushes on NP surfaces [46]. It can be predicted theoretically that lateral phase separation of two different polymer brushes on surfaces occurs in a marginally good nonselective solvent if both chains are of nearly equal or only slightly asymmetric in length. If one polymer species becomes larger, the smaller polymers form domains in a bottom layer close to the surface and the top layer is composed exclusively of the longer stretched polymer [47]. This predicted behavior has been confirmed experimentally [48].

Because the topology of separated polymer brushes on surfaces depends so strongly on the architecture of the polymeric species (i.e., the grafting density of both brushes and their degree of polymerization), the formation of well-defined mixed brushes on NP surfaces requires polymerization techniques that allow precise control over macromolecular properties. To this end, the use of macroRAFT agents for the formation of diblock copolymers with gold-binding TTC groups at the block junction has been suggested [49]. This approach is interesting because it implies that the ratio of grafting densities for the different blocks is always equal to one. Alternatively, the different brushes can be grafted to the NP surface as individual homopolymers through specific reactions between the homopolymer end groups and functional groups on the particle surface [50]. This could offer a handle for tuning the ratio of the two grafting densities by adjusting the polymer feed ratio. Another elegant and much-adapted method for preparing precisely tailored mixed polymer brushes is SI-ATRP followed by nitroxide-mediated radical polymerization (NMRP) from an asymmetric initiator that can be grafted to a surface of the particle and comprises initiation sites for both types of controlled radical polymerization techniques [51]. The two successive polymerizations lead to block copolymers grafted through their block junction. The resulting NPs show chain reorganization in response to a selective solvent environment that can lead to mobile and collapsed phases [51]. Employing this SI polymerization technique with asymmetric initiator, it can be shown by TEM that lateral microphase separation occurs in nonselective good solvents when the polymer molecular weight reaches a certain threshold value, and that a selective solvent leads to collapsed domains of the polymer species interacting unfavorably with the solvent [52, 53]. A systematic experimental study showed, from the analysis of TEM images, that the domain sizes grow strictly with the molecular weight of the grafted brushes, although the exact scaling behavior was dependent on whether the particles were drop-cast from a (nonselective) good or bad solvent [54]. A lower grafting density of mixed brushes also leads to larger domain sizes, until the grafting density reaches a

lower threshold value, below which no phase separation can be observed [55]. Lateral phase separation apparently leads to wedge-shaped separated domains if the curvature of the solid particles becomes large enough [56]. Phase separation is different in isolated nanohybrids compared with nanohybrids in self-assembled monolayers. For isolated hybrid particles, phase separation only occurs at the bottom close to the substrate, whereas interparticle brush interactions lead to extended phase-separated regions between neighboring particles [57].

The influence of the mode of attachment of different brushes was also investigated. Mixed brushes of PMMA and PS were grown from a flat silica surface by either SI conventional radical polymerization or successive ATRP (PMMA brush) and NMRP (PS brush) from a common asymmetric initiator for both techniques, attached to the surface with one grafting point. Conformational changes in grafted polymer chains were studied theoretically and experimentally by investigation of microphase separation after solvent exchange cycles with toluene and acetone. It was found that microphase-separated areas were larger for individually anchored PMMA and PS brushes. This effect was explained by density fluctuations of the different polymer species, which occur using this approach. Also, the memory measure (the probability that a specific domain re-forms after one cycle) was smaller for diblock copolymers grafted at their block junction. This was an indication that local fluctuations in grafted polymer chains act as nuclei in the domain structure formation [58].

Randomly distributed mixed brushes of PS and PN^{i}PAAM on AuNPs can be obtained by in-situ reduction of a gold salt precursor in the presence of RAFT homopolymers [59]. The presence of both types of polymers on the AuNPs can be demonstrated using NMR and infrared spectroscopy. When thin films of the composite material are prepared via hydrophilic Langmuir–Blodgett transfer, a more hydrophobic surface is obtained than with hydrophobic transfer, as shown from contact angle measurements after depositing a water drop on both surfaces. The authors concluded that this phenomenon might be indicative of phase separation of the two distinct polymer species on the NP surface during Langmuir–Blodgett assembly [59]. Detailed investigations into the behavior of mixed brushes can be undertaken when the polymers are grafted to a flat surface, which allows investigation via AFM [60]. Again, conformational changes in the polymer brushes allow the surface to adapt to its solvent environment, but it is interesting to notice that these conformational transitions can be kinetically locked when long enough chains cover shorter ones and thus prevent their swelling by a selective solvent [60].

For both cases where mixed brushes are randomly distributed over the surface or grafted as diblock copolymers at their block junctions, it was shown that the chain conformations can flexibly adapt to global changes in the environment. These observations were made by studying mixed brushes on NPs and lead to the question of whether such phenomena can be made useful for NP assembly [61]. When mixed brushes of thiol-terminated poly(ethylene glycol) (PEG) and PMMA from SI-ATRP are present on large (42 nm) gold nanocrystals, the hybrid particles proved stable as unimers in common solvents for both brushes (DMF, chloroform, DMSO). However, when the solvent was changed by addition of water and

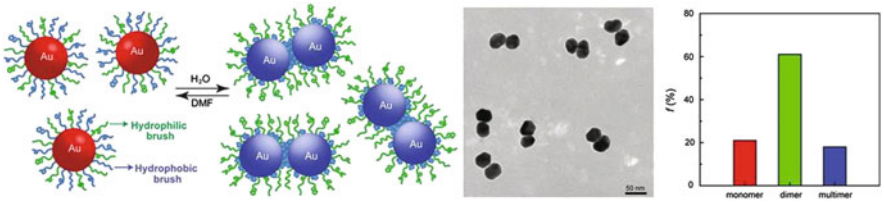

Fig. 4 *Left*: Proposed mechanism of dimerization upon solvent exchange to a selective solvent. *Center*: TEM image showing AuNP dimer structures. *Right*: Histogram showing the fraction of monomeric, dimeric, and multimeric AuNP species. Adapted with permission from [61]. Copyright 2011 American Chemical Society

subsequent dialysis, these nanohybrids aggregated, probably as a result of formation of hydrophobic domains of collapsed PMMA chains that act as contacting areas for different particles. Interestingly, NP assembly led to a huge proportion (>60%) of NP dimers. It was speculated that this is caused by depletion of PEG brushes from the dimer junction. The resulting accumulation of PEG brushes in the noncontacting areas leads to stabilization of the dimer structures (Fig. 4). This explanation is consistent with the observation that an increase in the PMMA fraction (PMMA:PEG ratio increase from 4:3 to >5:1) results in the formation of larger multimers upon addition of the selective solvent water [61].

Assemblies of nanocomposites into larger vesicular structures comprising several particles with mixed brushes can also be realized: AuNPs (14 nm) and nanorods (aspect ratio 4:1) were covered with thiol-terminated PEG (grafting-to) and thiol-terminated ATRP initiator, which allowed the growth of PMMA and PMMA-*stat*-poly(vinylpyridine) (PVP). Film rehydration of these nanocomposites led to vesicular structures. These structures were shown to decompose under heat or decreased pH, since vinylpyridine renders the system pH-responsive. In the case of nanorods, decomposition can be triggered with near-infrared radiation [62]. These features render this system promising for delivery and controlled release of therapeutic agents [63, 64].

4 Linear Diblock Copolymers and Random Copolymers

As a result of the general immiscibility of different homopolymers, diblock copolymers exhibit an inherent tendency to phase-separate and can therefore form a range of ordered structures in solution and in the molten state. Thus, there has been a lot of research using diblock copolymers in conjuncture with NPs and aiming to use these polymers as templates to form tailored NP arrangements. Block copolymers are attractive in the realm of nanocomposites because each of the two blocks can be employed for distinct functions. For example, for block copolymers grafted to IONPs, the inner block can be used as an attachment site for the incorporation of chemical tags, while the outer block provides solubility in the respective dispersant

[65]. Alternatively, block copolymers can be designed such that one entire block induces NP formation through gold salt reduction and shielding of the formed NP surface, and the second block provides colloidal stability. Following this idea, block copolymers of *N*,*N*-diemthylaminoethyl methacrylate (DMAEMA) and 2-(methacryloyloxy)ethyl phosphorylcholine (MPC) were prepared by ATRP. Addition of $HAuCl_4$ resulted in the accumulation of gold close to the DMAEMA repeating units as a result of formation of salt bridges. The (unprotonated) tertiary amine then acts as a reduction agent, which induces AuNP formation. Nanohybrids with an inner shell of PDMAEMA and an outer shell of PMPC are thus formed. Away from its isoelectric point, the PMPC layer imparts solubility to the nanocomposites. It was also shown that there is an optimum PDMAEMA block length for obtaining well-defined spherical AuNPs with reasonably narrow particle size distributions [66].

A more recent work employed the concept of gold salt reduction by one entire block of a block copolymer in an even more sophisticated fashion. Polymers comprising hydrophilic and hydrophobic blocks were used to coat AuNPs, which allowed growth of a gold nanoshell around these hybrid particles [67]. This became possible by introducing phenol side chain moieties into the hydrophilic block, which at basic pH were effective reducing agents for $KAuCl_4$, producing the gold shells. The hydrophobic blocks act as spacers in this case, which allows tuning of the thickness of the obtained nanogap between the gold core and shell, and also permits introduction of Raman tags by copolymerization with a functional monomer. The block that interacts with the NP surface is not necessarily chemically bound; adsorption of copolymers on NPs can lead to uniform polymer films [68]. It was demonstrated that hydrophobically functionalized AuNPs can be incorporated into micelles from polystyrene-*block*-poly(acrylic acid) (PS-*b*-PAA) copolymers by inducing micelle formation through addition of a selective solvent (water) and subsequent crosslinking of the outer shell of the micelle [69], or by cooling the solution to slowly decrease the critical micelle concentration [70]. In general, large excess of diblock copolymer (which can be separated after NP encapsulation) and a relatively large diameter of the NP ($>$10 nm) are necessary to avoid the incorporation of multiple NPs into one micelle. This has been observed for small NPs ($<$10 nm), which act as solutes swelling the micelle core [71]. In fact, the number of small NPs contained in a micelle can be controlled by adjusting the ratio of particles and block copolymers, with a higher average number of incorporated NPs being obtained as their relative proportion in the reaction mixture increases [72].

Triggered assembly of temperature-responsive diblock copolymers was used by McCormick and coworkers for colloidosome formation [73]. Block copolymers of DMAEMA and N^{i}PAAM were prepared by RAFT polymerization. Heating of a block copolymer solution induced reversible vesicle formation as a result of the collapse of the PN^{i}PAAM block. Addition of $NaAuCl_4$ to the assembled block copolymer solution at a fixed ratio at 50°C led to incorporation of gold salt in the vesicles. The tertiary amine group of the DMAEMA repeating unit triggered gold reduction and AuNP formation. Interestingly, the vesicular structure was fixed after cooling and did not dissociate into monomeric block copolymers, as observed

before AuNP formation [73]. In addition, the morphology of the self-assembled structures can be varied from simple micelles, mixtures of worm-like micelles and spherical micelles, and vesicles by adjusting the degree of polymerization of the temperature-responsive PN^{i}PAAM block in the preceding RAFT polymerization [74]. Preformed NPs can be incorporated into self-assembled solution structures of block copolymers depending on the specific interactions between the NP surface and both blocks. The NP–block copolymer interaction can, for example, lead to NPs being incorporated into micelle cores, although the constituting block copolymer alone forms vesicles. This is so because NP incorporation into the solvophobic phase can reduce the polymer stretching penalty in the self-assembled structures formed [75]. This point is further illustrated in a study by Park and coworkers [76], which showed that PS-coated quantum dots were incorporated into the PS domain of micelles formed from PS-*b*-PAA polymers. On the other hand, when alkyl-coated particles were employed, they formed a layer between the PS–PS interface [77]. This was shown to occur because the alkyl–PS interaction is the least unfavorable interaction and the incorporation of a NP layer reduces polymer stretching [76]. Thus, two NPs with different surface chemistries can be incorporated at different positions in the polymer matrix. The NP–copolymer interaction can also be tuned such that the NPs assemble at the PS–PAA interface of the micelles formed (by carefully choosing the surface chemistry of the NP) [78]. Hence, layered co-assemblies can be obtained with two types of particles located at the PS–PS and PS–PAA interfaces, resulting in different radial positions for the individual NPs (Fig. 5).

We have seen so far that enthalpic interaction parameters are often crucial in controlling the position of NPs in block copolymer assemblies [69–72, 74–78]. Nevertheless, it has been shown impressively that the contribution of entropy to the free energy can become important in controlling the position of NPs in vesicular structures [79]. The co-assembly of NPs decorated with polystyrene-*block*-poly (ethylene oxide) (PS-*b*-PEO) copolymers and free (not surface-bound) block copolymers of the same type leads to vesicles with the NPs being incorporated in the (solvophobic) PS domain. Interestingly, depending on the number of monomeric

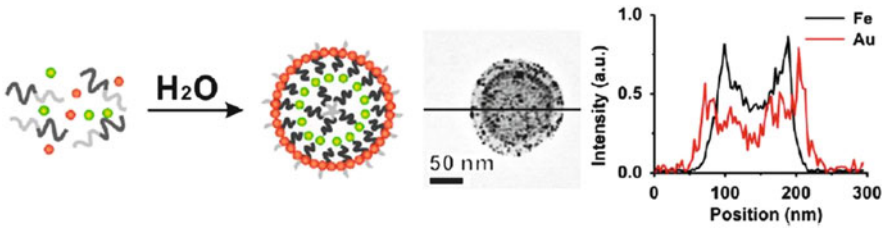

Fig. 5 Solvent-induced formation of layered assemblies from block copolymers of PAA and PS and AuNPs functionalized with mercaptoundecanol as well as IONPs functionalized with oleic acid. The AuNPs (*red*) are located at the PS–PAA interface, while the IONPs (*green and yellow*) are located at the PS–PS interface. The *graph* shows two different radial positions for the distinct NP species. Adapted with permission from [78]. Copyright 2013 American Chemical Society

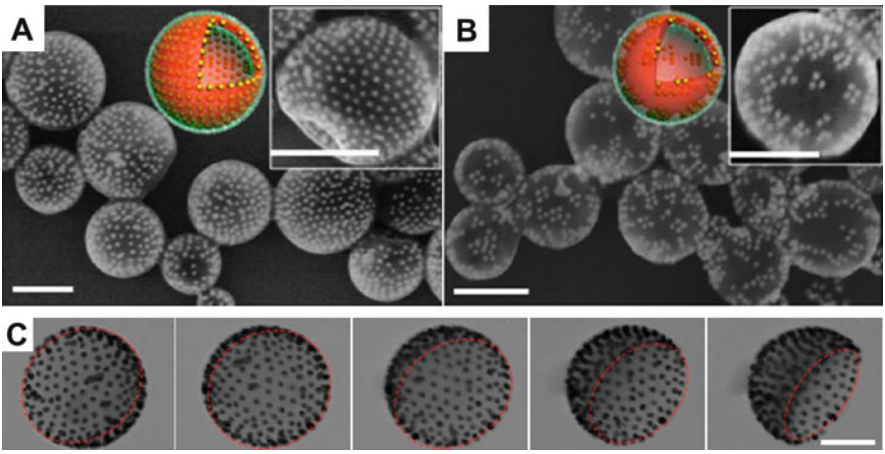

Fig. 6 (**a**, **b**) SEM images showing AuNPs grafted with block copolymers incorporated in vesicles and evenly distributed in one layer (**a**) or partly separated in clusters in this layer (**b**). (**c**) TEM images at different tilt angles revealing fully separated AuNPs in one hemisphere of the vesicle. *Scale bars*: 200 nm (**a**, **b**) and 100 nm (**c**). Adapted with permission from [79]. Copyright 2014 American Chemical Society

repeating units in the two blocks for both free and bound block copolymers, the NPs were either evenly distributed over the entire PS layer or they were separated. This separation led to an accumulation of NPs in some areas, leading to "patchy" vesicles, or – in cases of strong separation – to an accumulation on one hemisphere (and depletion on the other), leading to Janus-type structures (Fig. 6).

The concept of block copolymers acting as templates that can host NPs at defined locations can also be adopted to produce thin films. Thus, block copolymers, which show phase separation in the molten state, can be used as matrices for selective incorporation of particles. Depending on the block composition, and the temperature-dependent block interaction, phase separation can lead to different nanostructured morphologies [80]. However, we restrain ourselves here to discussion of the most common type of phase separation, lamellar phase separation, as an illustrative example. The lamellar type of phase separation has the advantage that, as a result of its symmetry, it facilitates computations towards the prediction of NP localization in diblock copolymer hosts. A theoretical study evaluating NP distribution in copolymer melts found that neutral NPs lead to a Gaussian distribution centered at the lamellar interfaces, whereas strongly selective NPs are incorporated in the preferred domain, with a Gaussian distribution centered at the middle of this domain [81]. There could also be intermediate situations in which Gaussian distributions with distinct shoulders are observed. Generally, large degrees of polymerization in the diblock copolymer, and therefore a high degree of domain segregation, were shown to lead to narrow particle distributions in this theoretical work [81], a finding that is, however, contrary to an experimental study investigating this effect [82].

Depending on the wetting behavior of the two blocks of the block copolymer with the surface, thin films can show phase separation that is either parallel or perpendicular to the surface. If the surface comprises equal wettability for both blocks, this usually results in perpendicular phase separation. This effect can be nicely demonstrated by comparing two types of NPs, one of which is selective and one of which is neutral for a common block copolymer of PS and PMMA. It can be demonstrated experimentally that selective AuNPs locate inside the favorable block domain, whereas neutral NPs are located at the domain interfaces (see Fig. 7) [83], fully consistent with theory [81] and other experimental studies [84, 85]. It was furthermore shown by cross-sectional TEM that selective NPs are distributed throughout the respective domain, but within the entire film thickness, whereas neutral NPs reside preferentially close to the surface–air interface for entropic reasons [83]. The attraction of NPs to the surface of the substrate thus induces a change in the surface wettability properties and results in conversion from parallel to perpendicular phase separation when the amount of neutral NPs is high enough. A similar transition of block copolymer orientation after addition of NPs to the system has also been observed by others, employing a different system comprising PS-*b*-PVP copolymer together with alkyl-coated CdSe particles [86, 87]. To take full advantage of the periodical features present on the surface of phase-separated thin films, one could also choose to further swell specific domains with selective solvents prior to the addition of particles [88] or to permanently fix the phase separation by photo-crosslinking [89].

By adding NPs to phase-separating block copolymer systems, one may also face phenomena resulting from interparticle interactions, which are often neglected by theory: When lamellar phase separation is used to introduce magnetic NPs

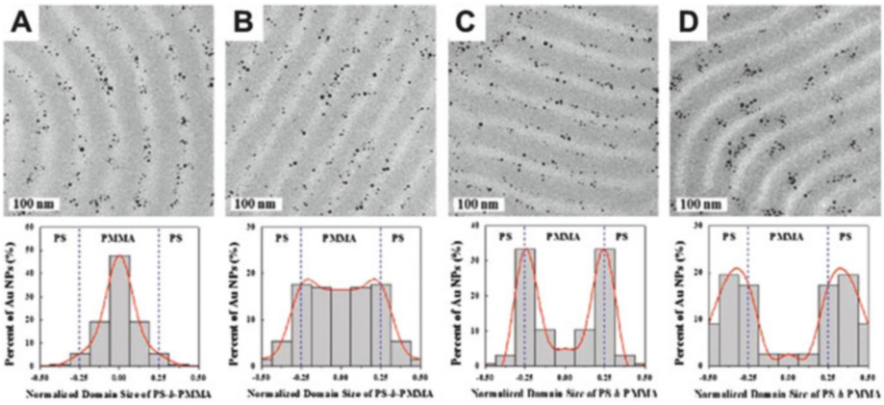

Fig. 7 *Top row*: TEM images showing the lamellar phase separation of a PS-*b*-PMMA polymer perpendicular to the substrate surface (PS domains were stained with RuO_4 and appear darker) and the distribution of AuNPs modified with four different polymeric ligands. The fraction of styrene increases from **a** to **d**. *Bottom row*: Particle distribution in the block copolymer domains for AuNPs coated with the four different polymers. Adapted with permission from [83]. Copyright 2011 American Chemical Society

functionalized with PMMA into the PMMA domain of a PS-*b*-PMMA copolymer, the incorporation can occur only at small NP concentrations. When the NP concentration is high enough, the polymer-coated NPs tend to form particle aggregates that are too large to be taken up inside one block domain, and therefore block copolymer assembly around these aggregates is observed [90]. A different scenario that can be observed upon increasing the NP concentration is an NP-induced phase transition. An interesting mechanism leading to phase transition in block copolymers has been described by Kramer and coworkers [91]. When NPs, which prefer to locate at block interfaces, were added with increasing concentration, the authors found that initially the domain size in lamellar phase-separated block copolymers decreased. This behavior was rationalized by strong segregation theory, predicting a scaling of domain thickness proportional to the block copolymer interfacial energy, which is decreased by addition of neutral NPs locating at the copolymer interfaces. Further increase in the NP concentration led to a lamellar-to-bicontinous transition, as shown for AuNPs selective for an interface with two different surface coatings. The effect of the molecular weight of the block copolymer matrix on the phase transition was also studied and it was found that matrices with higher molar masses required smaller NP concentrations for phase transition [91].

5 Linear Triblock Polymers

By applying triblock terpolymers as templates for the in situ formation of NPs, it is possible to introduce even more information into a linear polymer by using the different blocks for distinct functions. For example, two outer blocks can be chosen such that the resulting polymer has a tendency to self-assemble into specific solution structures, while the inner block can comprise binding sites for NPs [92, 93]; alternatively, one outer block can provide these binding sites and the other two blocks can provide amphiphilicity [94, 95]. Such triblock terpolymers are, for example, accessible through consecutive RAFT [92, 93] or ATR [94, 95] polymerizations. When an inner block of either PMAA [92] (providing attachment sites for the complexation of an iron salt precursor) or PDMAEMA [93] (providing attachment sites for tetrachloroauric acid) is sandwiched between outer blocks of PS and poly[oligo(ethylene glycol) methacrylate] (POEGMA), the polymers can be used to organize inorganic NPs into different patterns. Polymerization-induced self-assembly was employed in both of these studies; that is, the respective block copolymer precursors were used as macroRAFT agents in chain extension polymerizations with styrene in methanol, under which conditions polymeric NPs were formed. The two different inorganic precursor salts could then be introduced into the respective middle block of the triblock terpolymers, and inorganic particle formation could be triggered by adding base to form IONPs [92] or reduction agent to form AuNPs [93]. Depending on the degree of polymerization of styrene, this system can be tuned to form micelles, rods, and vesicles as hosts for inorganic NPs [92]. The polymers therefore encode these different solution structures and at the same time

carry information about where the inorganic NPs will be placed in the resulting nanohybrid assembly structures.

The studies mentioned above first assemble specifically designed polymers and then induce NP formation after assembly formation. In principle, however, it should be possible to first decorate inorganic NPs with a polymer to create amphiphilic hybrid particles, which can then assemble into a variety of structures. This has been realized by Eisenberg and coworkers [96]. Their approach used triblock polymers made by two successive ATR polymerizations of first styrene and then vinylpyridine, starting from a chloride-terminated PEG macroinitiator. The resulting PEG-*b*-PS-*b*-PVP polymers were used to cover AuNPs and PdNPs via attachment through the PVP block. The obtained hybrid particles had amphiphilic character and tended to assemble into micellar structures after addition of water to their dispersions in THF. The self-assembled structures revealed (by TEM characterization) NPs with defined location at the surface of the micellar core, which occurred in darker contrast as a result of the high electron density in the PS block. The defined NP position resulted from the covalent attachment of the separating blocks. The hydrophilic PEG block could effectively stabilize these micellar structures in the hydrophilic environment at high enough grafting densities [96].

Even higher precision in the formation of nanocomposites can be achieved by the ambitious procedure of NP monofunctionalization [97]. Liu and coworkers indeed found that small AuNPs can be functionalized with only a single macromolecule, a triblock terpolymer [98]. The authors used a macroRAFT agent with PEO in its RAFT leaving group ("R group") to successively polymerize glycidyl methacrylate (GMA) and styrene. The middle PGMA block was used to introduce lipoic acid, which acts as an anchor for gold surfaces via its dithiolane moiety. By analyzing the nanohybrids of this polymer with AuNPs via size-exclusion chromatography (SEC) and thermogravimetric analysis (TGA), it was concluded that indeed only one macromolecule attaches to AuNPs with diameters of ~2.0, ~2.9, and ~3.8 nm. Monofunctionalization was, however, not observed for AuNPs of ~4.9 nm, strongly suggesting a size selectivity for this stoichiometric functionalization. The nanocomposites with one macromolecule per inorganic particle were decorated with a PEO and a PS chain (the outer blocks of the initial triblock polymer) and can therefore be considered as true amphiphilic particles. The assembly of these nanohybrid particles into vesicles and micelles, depending on the packing parameter (which can be controlled by macromolecular design), has been demonstrated (Fig. 8) [98].

In addition to the above-discussed cases of triblock terpolymers, linear triblock polymers can also take the form of ABA copolymers. A recent study [99] employed a symmetric ATRP macroinitiator with a PEG linker between the two initiation sites. ATR copolymerization of diethylenegylcol methylmethacrylate (DEGMMA) and diethyleneglycol ethylmethacrylate (DEGEMA), together with a comonomer for fluorescent labeling, permitted the formation of outer blocks with defined lower critical solution temperature (LCST). Silica NPs were surface-functionalized by SI-ATRP with polymers of different compositions of DEGMMA and DEGEMA to tune the LCST of the surface-grafted polymer and another comonomer as

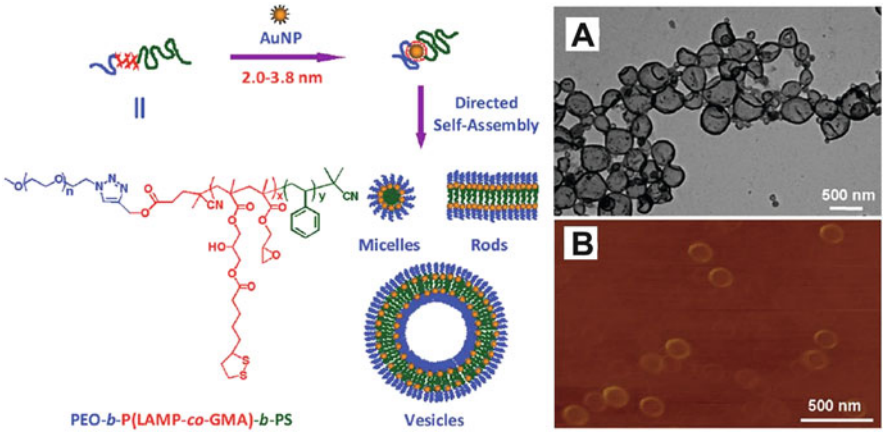

Fig. 8 *Left*: Strategy employed for the monofunctionalization of AuNPs with one macromolecule. *Right*: High resolution TEM (**a**) and AFM (**b**) images of the vesicular assembly structures obtained from these nanohybrids. Adapted with permission from [98]. Copyright 2012 American Chemical Society

fluorescent tag. The fluorescent labels were introduced to study the spatial relation of the surface-modified SiNPs with the outer blocks of the triblock ABA copolymer. When the polymer immobilized on the SiNP surface had a similar LCST as the outer blocks of the triblock copolymer, mixtures of both species formed gels at a temperature above their common LCST. In these gels, the NPs were localized in micellar compartments of the collapsed outer A blocks of the ABA copolymer. Gel formation was a result of the bridging of (soluble) PEG chains (B block of the ABA copolymer) between the collapsed entities. When the SiNPs were modified with a polymer of higher LCST than that of the outer block of the triblock copolymer, gels were formed at temperatures intermediate between the two LCSTs and SiNPs were not incorporated into the collapsed micelles. Careful manipulation of the properties of the surface-bound polymers therefore allows control of the location of inorganic NPs in organic polymer gels [99].

6 Linear Multiblock Polymers

RAFT polymerization is unique among the most prominent RDRP techniques because the inherently bifunctional TTC group can be employed in RAFT-type chain transfer agents. As a result of this bifunctional nature, the TTC moiety can be easily incorporated into the backbone of linear multifunctional RAFT agents [100, 101] or cyclic RAFT agents [102], both of which permit the formation of multiblock polymers with narrowly distributed block lengths. In such systems, the RAFT mechanism causes a continuous redistribution of all blocks and RAFT

groups during polymerization and this results in remarkably narrow ideal block distributions [103]. Consequently, such macromolecules are relatively well defined and can thus be used as the tailored organic part of nanohybrids with inorganic particles. For AuNPs, this polymer comprises TTC groups as gold attachment points in its backbone [104]. Another advantage of these systems is that multiblock copolymers can be obtained by only two successive polymerizations. Such multiblock copolymers can be useful, as shown by Du et al., who suggested that amphiphilic RAFT multiblock copolymers of styrene and vinylpyridine can be used for the interfacial assembly of AuNPs, gold nanorods, and AgNPs at liquid–liquid interfaces [105]. The authors did not show, however, whether the TTC groups are maintained in the multiblock copolymers after treating them with $NaBH_4$ during the in situ synthesis of AuNPs and AgNPs.

When the covalently linked blocks of a multiblock polymer are made of N^{i}PAAM monomer, the resulting polymeric material is water soluble and can therefore be brought directly into contact with AuNPs from the citrate reduction. Nanohybrids produced by this method were analyzed by TEM, which showed particles that assembled in hexagonal two-dimensional patterns with constant minimum spacing between the gold cores; absolutely no particle stacking was observed [44]. This indicates that the gold cores were not crosslinked by the multifunctional RAFT polymer, a result that was confirmed by SEC analysis. The binding mode of this polymer on the surface of this type of AuNP could be revealed in even more detail: The spacing between the gold cores was analyzed systematically for different multiblock polymers of N^{i}PAAM and compared with the data (see Sect. 1, Fig. 3) obtained for linear polymers of N^{i}PAAM with only one TTC group on the ω-end of the polymeric chain. It was found that gold core spacings were distinctively smaller and almost constant when multifunctional RAFT polymers with varying block numbers and degrees of polymerization were employed for surface functionalization reactions with these AuNPs. This leads to the conclusion that this type of polymer attaches to AuNPs from citrate reduction in a multivalent fashion via its multiple TTC groups, meaning that these macromolecules wrap around the AuNPs and form polymer loops on the NP surface [44].

Disclosing the binding motif of multiblock RAFT polymers on AuNPs from citrate reduction raises the question of whether the polymer binding can vary for different types of AuNPs. It is known that AuNPs from the two-phase Brust–Schiffrin synthesis can assemble into spherical particle networks when treated with low molecular weight crosslinking agent [106, 107]. When tetraoctylammonium bromide-capped AuNPs from this two-phase method are functionalized in toluene dispersion with multiblock RAFT polymers of styrene, the formation of spherical AuNP assemblies can be observed by TEM (Fig. 9) [108]. It can be concluded from these TEM images that the particle density inside

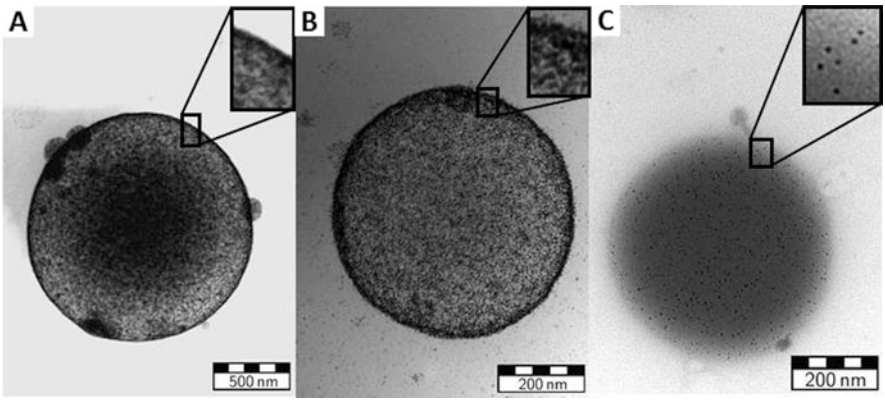

Fig. 9 (**a**–**c**) TEM images of AuNP networks obtained by treating TOAB-capped AuNPs in toluene with multifunctional RAFT polymers of styrene. The degree of polymerization of the polymeric particle linker increases from **a** to **c**. Adapted with permission from [108]. Copyright 2013 American Chemical Society

these assemblies decreases when polymers with increasing degree of polymerization are employed in NP functionalization reactions. By AFM characterization, it was possible to determine the three-dimensional shape of these structures after drop-casting from dispersion and solvent evaporation. It was found that these objects partly preserve a globular structure, which is indicative of NP crosslinking, as bonded particles are prevented from slipping when interconnected. The spherical superstructures can be further agglomerated into chain-like structures by addition of a non-solvent [104].

7 Branched Polymeric Architectures

Branched polymers are fundamentally different from linear polymers, which were discussed in previous sections: Polymers of linear topology contain two end groups, whereas multiple end groups are present in branched architectures, which allows incorporation of multiple functional groups into macromolecules of globular shape. Branched polymers can therefore be considered as promising macromolecular NP linkers. The branching points can be statistically distributed over the macromolecules (hyperbranched polymers, HBPs), occur strictly regularly leading to generational structures (dendrimers), or branches can be joined at a common core (star polymers).

Branched polymers can still attach to surfaces via one or multiple branches. It is possible to attach an HBP to an inorganic particle with only one of its branches if an ATRP initiator is immobilized on a surface, followed by polymerization of an initiator–monomer [109]. HBP with multiple anchor sites for NPs was prepared by Fredericks and coworkers [110], who produced hyberbranched RAFT polymer by copolymerization with a difunctional monomer. The RAFT agent was of the TTC type and also contained an alkyne moiety in its RAFT leaving group; both functional groups are known to attach to gold surfaces. Addition of these polymers to AuNPs from citrate reduction resulted in the formation of nanohybrid particles with unbound TTC and alkyne groups on their surfaces. These available functional groups could be used for the attachment of citrate-capped AuNPs, resulting in crosslinked AuNP nanoassemblies. In a subsequent study [111] by the same authors, it was shown that the structure of these nanoassemblies varies with the macromolecular architecture of the HBP: With low numbers of branches (and consequently a low number of anchoring sites for gold), the nanoassemblies showed a plate-like morphology, whereas for a higher number of branches, globular assemblies with densely packed AuNPs were found. Because the approach introduced in these studies allows the attachment of further particles to a scaffold of nanohybrid particles, it could also allow the attachment of particles of a different type to this scaffold architecture, leading to hierarchical multicomponent nanostructures. Such nanostructures can be realized using this approach by treating larger (48 nm) citrate-stabilized AuNPs with HBP to create nanohybrids acting as the scaffold, and then adding smaller (15 nm) citrate-capped AuNPs after purification of the initial nanohybrids [112]. The approach resulted in the formation of planet–satellite nanostructures; varying the stoichiometric ratio of the two types of inorganic particles employed could control the average number of satellite particles in these arrangements.

Another key parameter of such multicomponent particle architectures is the average interparticle distance. This parameter can be tightly controlled if RAFT star polymers with TTC groups on their exterior are used to interconnect two different types of AuNPs, as shown by Rossner and Vana [113]. In this study, particles from citrate reduction (14 nm) were treated with four-arm star polymers of N^{i}PAAM of varying molecular weight to form nanohybrid scaffold architectures. It was shown by TEM analysis that the thickness of the coating polymer shell increased strictly with increasing star polymer molecular weight. The purified star polymer nanocomposites could then be treated with AuNPs from the two-phase Brust–Schiffrin method to obtain planet–satellite arrangements with set planet–satellite distances (Fig. 10).

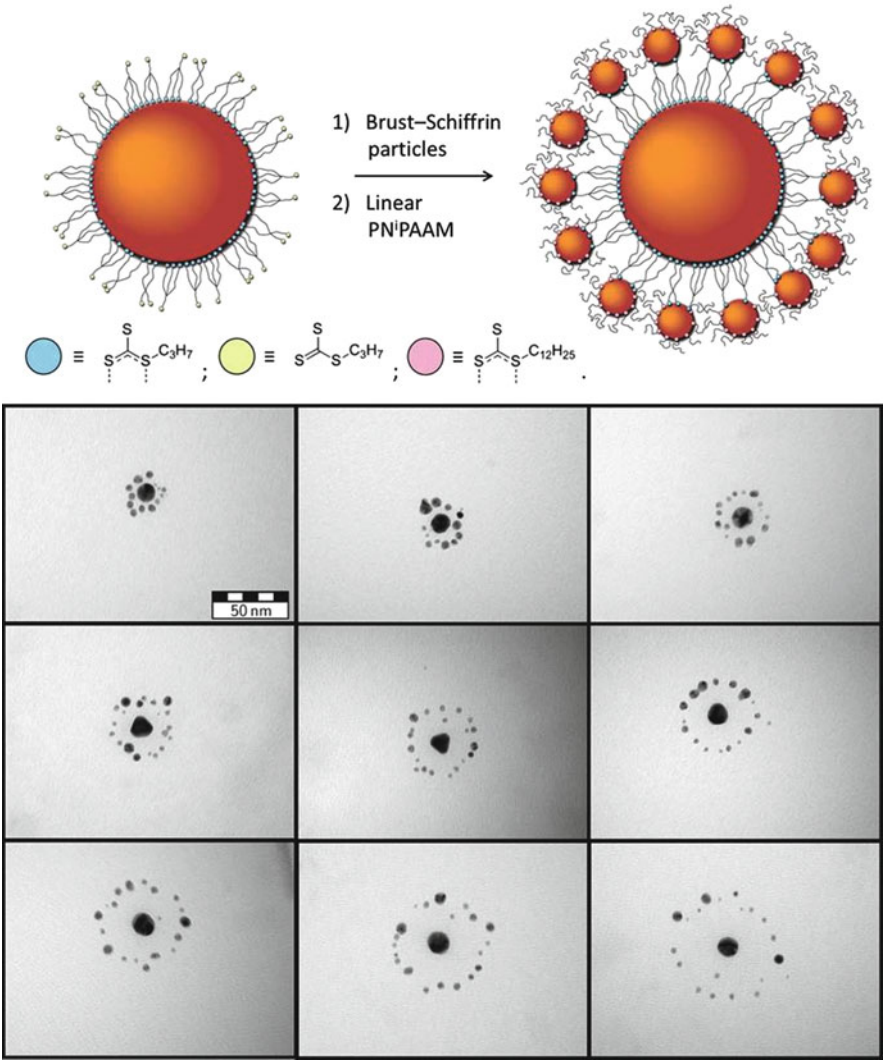

Fig. 10 *Top*: Synthetic scheme for the fabrication of planet–satellite nanostructures with star polymers acting as particle linkers, and linear polymers to provide colloidal stability. *Bottom*: TEM images of planet–satellite nanostructures. The average molecular weight of the linking star polymers increases from *left* to *right* and from *top* to *bottom*. Adapted with permission from [113]. Copyright 2014 Wiley-VCH Verlag GmbH & Co. KGaA, Weinheim

8 Conclusion

As indicated by the title of the chapter, we have restricted ourselves to a discussion of polymeric systems realized via controlled radical polymerization. There is a plethora of articles closely related to the research presented in this chapter; however, different techniques were employed to produce the polymers used for these studies. In order to stick with the idea of this chapter, we have not discussed such papers. One example that illustrates this point is work from Shenhar, Müller, and coworkers [114, 115]. These authors used anionic polymerization to prepare phase-separating block copolymers of PS and PMMA for incorporation of NPs into thin films. They employed interparticle interactions intentionally to achieve even more control of particle structuring in block copolymer thin films than in the examples given in Sect. 3: When NPs are used that interact unfavorably with both block copolymer domains, but less unfavorably with one domain, the NPs are incorporated into this domain but still have a tendency to separate, leading to hexagonally close-packed assemblies of NPs inside a specific host domain. It can be shown that the average distance between particles in these hexagonal arrangements can be controlled by tuning the length of the ligand attached to the NPs, a principle which we know from the discussion in Sect. 1.

We have seen in Sect. 1 that nanocomposites with distinct functional groups repeatedly presented on the surface can be used for specific interactions, which can lead to applications such as targeting of carcinoma cells. The length of the surface-bound polymer can be used to encode interparticle spacing in two- and three-dimensional assemblies, with possible applications in material science. Also, the scaling of interparticle distance with the molar mass of surface-anchored polymer contains information about the conformational state of the polymer at the surface. The set of parameters, which determines the architecture of polymers in nanocomposites, can be drastically expanded when two types of linear homopolymers are used instead of one (Sect. 2). In such situations, phase separation phenomena can be observed on the surfaces of colloidal particles, and we have seen how this phase separation can be modulated by the design of the employed macromolecules. The tendency of two different polymers to separate can also be exploited by covalently linking two immiscible homopolymers (i.e., by preparing diblock copolymers, as described in Sect. 3). By carefully adjusting its architecture, this type of polymer can be used to precisely control the location of inorganic NPs in a molten or solution state. Related to this is the case of triblock polymers presented in Sect. 4, whereby additional functionality can be imparted to the macromolecules through introduction of the third block. By further increasing the block number (i.e., creating multifunctional polymers, as discussed in Sect. 5), it is possible to encode polymer loops at surfaces and also to achieve NP crosslinking. The branched polymeric architectures presented in Sect. 6 can also be considered as multifunctional polymers, but with a different topology from linear multiblock polymers. It was shown that it is possible to accurately tune the distances between

two different types of NPs by adjusting the size of the branched polymeric linker through controlled radical polymerization.

The work done during the last decade and reflected in the literature summarized in this review therefore suggests that specifically designed macromolecules contain information that can be translated to the structure of nanohybrids and self-assembled structures. The encoding of this information with macromolecules becomes possible through macromolecular design by means of controlled radical polymerization. Thus, macromolecular design via controlled radical polymerization can be considered as a versatile programming language [116, 117] to guide nanocomposite formation and assembly.

The huge variety of defined nanostructures and materials that can be fabricated via controlled radical polymerization techniques will probably find applications in a wide field of different research directions. The possibility of combining several building units in one device will enable materials scientists to implement multiple levels of stimuli-responsiveness for the construction of smart materials. Research in biomedicine can be expected to benefit from the ability to generate defined nanopatterned surfaces that can play a central role in biophysical investigations. Also, the potential to create precisely defined confined environments could lead to nanocontainers as delivery vehicles, theranostic agents, or artificial enzymes.

References

1. Velev OD, Gupta S (2009) Adv Mater 21:1897–1905
2. Li D, Jones GL, Dunlap JR, Hua F, Zhao B (2006) Langmuir 22:3344–3351
3. Takara M, Toyoshima M, Seto H, Hoshino Y, Miura Y (2014) Polym Chem 5:931–939
4. Richards S-J, Gibson MI (2014) ACS Macro Lett 3:1004–1008
5. Lowe AB, Sumerlin BS, Donovan MS, McCormick CL (2002) J Am Chem Soc 124:11562–11563
6. Garcia MA (2011) J Phys D Appl Phys 44:283001
7. Duwez A-S, Guillet P, Colard C, Gohy J-F, Fustin C-A (2006) Macromolecules 39:2729–2731
8. Blakey I, Schiller TL, Merican Z, Fredericks PM (2010) Langmuir 26:692–701
9. Slavin S, Soeriyadi AH, Voorhaar L, Whittaker MR, Becer CR, Boyer C, Davis TP, Haddleton DM (2012) Soft Matter 8:118–128
10. Ulman A (1996) Chem Rev 96:1533–1554
11. Pujari SP, Scheres L, Marcelis ATM, Zuilhof H (2014) Angew Chem Int Ed 53:6322–6356
12. Huebner D, Koch V, Ebeling B, Mechau J, Steinhoff JE, Vana P (2015) J Polym Sci Part A Polym Chem 53:103–113
13. Gibson MI, Danial M, Klok H-A (2011) ACS Comb Sci 13:286–297
14. Freese C, Gibson MI, Klok H-A, Unger RE, Kirkpatrick CJ (2012) Biomacromoleules 13:1533–1543
15. Blakey I, Merican Z, Thurecht KJ (2013) Langmuir 29:8266–8274
16. Fasting C, Schalley CA, Weber M, Seitz O, Hecht S, Koksch B, Dernedde J, Graf C, Knapp E-W, Haag R (2012) Angew Chem Int Ed 51:10472–10498
17. Álvarez-Paino M, Bordegé V, Cuervo-Rodríguez R, Muñoz-Bonilla A, Fernández-García M (2014) Macromol Chem Phys 215:1915–1924
18. Housni A, Cai H, Liu S, Pun SH, Narain R (2007) Langmuir 23:5056–5061

19. Toyoshima M, Miura Y (2009) J Polym Sci Part A Polym Chem 47:1412–1421
20. Spain SG, Albertin L, Cameron NR (2006) Chem Commun 2006(40):4198–4200
21. Lu J, Zhang W, Richards S-J, Gibson MI, Chen G (2014) Polym Chem 5:2326–2332
22. Li X, Bao M, Weng Y, Yang K, Zhang W, Chen G (2014) J Mater Chem B 2:5569–5575
23. Li J, Han C, Wu W, Zhang S, Guo J, Zhou H (2014) New J Chem 38:717–722
24. Celiz AD, Lee T-C, Scherman OA (2009) Adv Mater 21:3937–3940
25. Ohno K, Koh K, Tsujii Y, Fukuda T (2003) Angew Chem Int Ed 42:2751–2754
26. Ohno K, Morinaga T, Koh K, Tsujii Y, Fukuda T (2005) Macromolecules 38:2137–2142
27. Boyer C, Whittaker MR, Luzon M, Davis TP (2009) Macromolecules 42:6917–6926
28. Ohno K, Morinaga T, Takeno S, Tsujii Y, Fukuda T (2007) Macromolecules 40:9143–9150
29. Morinaga T, Ohno K, Tsujii Y, Fukuda T (2008) Macromolecules 41:3620–3626
30. Ohno K, Akashi T, Huang Y, Tsujii Y (2010) Macromolecules 43:8805–8812
31. Ohno K, Morinaga T, Takeno S, Tsujii Y, Fukuda T (2006) Macromolecules 39:1245–1249
32. Daoud M, Cotton JP (1982) J Phys (Paris) 43:531–538
33. Dukes D, Li Y, Lewis S, Benicewicz B, Schadler L, Kumar SK (2010) Macromolecules 43:1564–1570
34. Choi J, Dong H, Matyjaszewski K, Bockstaller MR (2010) J Am Chem Soc 132:12537–12539
35. Choi J, Hui CM, Pietrasik J, Dong H, Matyjaszewski K, Bockstaller MR (2012) Soft Matter 8:4072–4082
36. Choi J, Hui CM, Schmitt M, Pietrasik J, Margel S, Matyjazsewski K, Bockstaller MR (2013) Langmuir 29:6452–6459
37. Rungta A, Natarajan B, Neely T, Dukes D, Schadler LS, Benicewicz BC (2012) Macromolecules 45:9303–9311
38. Akcora P, Liu H, Kumar SK, Moll J, Li Y, Benicewicz BC, Schadler LS, Acehan D, Panagiotopoulos AZ, Pryamitsyn V, Ganesan V, Ilavsky J, Thiyagarajan P, Colby RH, Douglas JF (2009) Nat Mater 8:354–359
39. Goel V, Pietrasik J, Dong H, Sharma J, Matyjaszewski K, Krishnamoorti R (2011) Macromolecules 44:8129–8135
40. Yockell-Lelièvre H, Gingras D, Vallée R, Ritcey AM (2009) J Phys Chem C 113:21293–21302
41. Karg M, Hellweg T, Mulvaney P (2011) Adv Funct Mater 21:4668–4676
42. Ohno K, Ma Y, Huang Y, Mori C, Yahata Y, Tsujii Y, Maschmeyer T, Moraes J, Perrier S (2011) Macromolecules 44:8944–8953
43. Moraes J, Ohno K, Gody G, Maschmeyer T, Perrier S (2013) Beilstein J Org Chem 9:1226–1234
44. Ebeling B, Vana P (2013) Macromolecules 46:4862–4871
45. Yockell-Lelièvre H, Desbiens J, Ritcey AM (2007) Langmuir 23:2843–2850
46. Wang Y, Yang G, Tang P, Qiu F, Yang Y, Zhu L (2011) J Chem Phys 134:134903
47. Wang J, Müller M (2009) J Phys Chem B 113:11384–11402
48. Jiang X, Zhong G, Horton JM, Jin N, Zhu L, Zhao B (2010) Macromolecules 43:5387–5395
49. Wang Z-L, Xu J-T, Du B-Y, Fan Z-Q (2011) J Colloid Interface Sci 360:350–354
50. Kotsuchibashi Y, Ebara M, Aoyagi T, Narain R (2012) Polym Chem 3:2545–2550
51. Li D, Sheng X, Zhao B (2005) J Am Chem Soc 127:6248–6256
52. Zhu L, Zhao B (2008) J Phys Chem B 112:11529–11536
53. Zhao B, Zhu L (2006) J Am Chem Soc 128:4574–4575
54. Bao C, Tang S, Wright RAE, Tang P, Qiu F, Zhu L, Zhao B (2014) Macromolecules 47:6824–6835
55. Bao C, Tang S, Horton JM, Jiang X, Tang P, Qiu F, Zhu L, Zhao B (2012) Macromolecules 45:8027–8036
56. Horton JM, Tang S, Bao C, Tang P, Qiu F, Zhu L, Zhao B (2012) ACS Macro Lett 1:1061–1065

57. Tang S, Lo T-Y, Horton JM, Bao C, Tang P, Qiu F, Ho R-M, Zhao B, Zhu L (2013) Macromolecules 46:6575–6584
58. Santer S, Kopyshev A, Donges J, Rühe J, Jiang X, Zhao B, Müller M (2007) Langmuir 23:279–285
59. Shan J, Nuopponen M, Jiang H, Viitala T, Kauppinen E, Kontturi K, Tenhu H (2005) Macromolecules 38:2918–2926
60. Ionov L, Minko S (2012) ACS Appl Mater Interfaces 4:483–489
61. Cheng L, Song J, Yin J, Duan H (2011) J Phys Chem Lett 2:2258–2262
62. Song J, Cheng L, Liu A, Yin J, Kuang M, Duan H (2011) J Am Chem Soc 133:10760–10763
63. Song J, Zhou J, Duan H (2012) J Am Chem Soc 134:13458–13469
64. Song J, Pu L, Zhou J, Duan B, Duan H (2013) ACS Nano 7:9947–9960
65. Basuki JS, Duong HTT, Macmillan A, Whan R, Boyer C, Davis TP (2013) Macromolecules 46:7043–7054
66. Yuan J-J, Schmid A, Armes SP, Lewis AL (2006) Langmuir 22:11022–11027
67. Song J, Duan B, Wang C, Zhou J, Pu L, Fang Z, Wang P, Lim TT, Duan H (2014) J Am Chem Soc 136:6838–6841
68. Marcelo G, Martinho JMG, Farinha JPS (2013) J Phys Chem B 117:3416–3427
69. Kang Y, Taton TA (2005) Angew Chem Int Ed 44:409–412
70. Chen HY, Abraham S, Mendenhall J, Delamarre SC, Smith K, Kim I, Batt CA (2008) ChemPhysChem 9:388–392
71. Kang Y, Taton TA (2005) Macromolecules 38:6115–6121
72. Kim B-S, Qiu J-M, Wang J-P, Taton TA (2005) Nano Lett 5:1987–1991
73. Li Y, Smith AE, Lokitz BS, McCormick CL (2007) Macromolecules 40:8524–8526
74. Smith AE, Xu X, Abell TU, Kirkland SE, Hensarling RM, McCormick CL (2009) Macromolecules 42:2958–2964
75. Hickey RJ, Haynes AS, Kikkawa JM, Park S-J (2011) J Am Chem Soc 133:1517–1525
76. Kamps AC, Sanchez-Gaytan BL, Hickey RJ, Clarke N, Fryd M, Park S-J (2010) Langmuir 26:14345–14350
77. Sanchez-Gaytan BL, Cui W, Kim Y, Mendez-Polanco MA, Duncan TV, Fryd M, Wayland BB, Park S-J (2007) Angew Chem Int Ed 46:9235–9238
78. Luo Q, Hickey RJ, Park S-J (2013) ACS Macro Lett 2:107–111
79. Liu Y, Li Y, He J, Duelge KJ, Lu Z, Nie Z (2014) J Am Chem Soc 136:2602–2610
80. Mai Y, Eisenberg A (2012) Chem Soc Rev 41:5969–5985
81. Matsen MW, Thompson RB (2008) Macromolecules 41:1853–1860
82. Chiu JJ, Kim BJ, Yi G-R, Bang J, Kramer EJ, Pine DJ (2007) Macromolecules 40:3361–3365
83. Yoo M, Kim S, Jang SG, Choi S-H, Yang H, Kramer EJ, Lee WB, Kim BJ, Bang J (2011) Macromolecules 44:9356–9365
84. Chiu JJ, Kim BJ, Kramer EJ, Pine DJ (2005) J Am Chem Soc 127:5036–5037
85. Li Q, He J, Glogowski E, Li X, Wang J, Emrick T, Russell TP (2008) Adv Mater 20:1462–1466
86. Lin Y, Böker A, He J, Sill K, Xiang H, Abetz C, Li X, Wang J, Emrick T, Long S, Wang Q, Balazs A, Russell TP (2005) Nature 434:55–59
87. He J, Tangirala R, Emrick T, Russell TP, Böker A, Li X, Wang J (2007) Adv Mater 19:381–385
88. Son JG, Bae WK, Kang H, Nealey PF, Char K (2009) ACS Nano 3:3927–3934
89. Tietz K, Finkhäuser S, Samwer K, Vana P (2014) Macromol Chem Phys 215:1563–1572
90. Xu C, Ohno K, Ladmiral V, Milkie DE, Kikkawa JM, Composto RJ (2009) Macromolecules 42:1219–1228
91. Kim BJ, Fredrickson GH, Hawker CJ, Kramer EJ (2007) Langmuir 23:7804–7809
92. Karagoz B, Yeow J, Esser L, Prakash SM, Kuchel RP, Davis TP, Boyer C (2014) Langmuir 30:10493–10502
93. Bleach R, Karagoz B, Prakash SM, Davis TP, Boyer C (2014) ACS Macro Lett 3:591–596
94. Duxin N, Liu F, Vali H, Eisenberg A (2005) J Am Chem Soc 127:10063–10069

95. Niu H, Zhang L, Gao M, Chen Y (2005) Langmuir 21:4205–4210
96. Azzam T, Bronstein L, Eisenberg A (2008) Langmuir 24:6521–6529
97. Krüger C, Agarwal S, Greiner A (2008) J Am Chem Soc 130:2710–2711
98. Hu J, Wu T, Zhang G, Liu S (2012) J Am Chem Soc 134:7624–7627
99. Hu B, Henn DM, Wright RAE, Zhao B (2014) Langmuir 30:11212–11224
100. Ebeling B, Vana P (2011) Polymers (Basel) 3:719–739
101. You Y-Z, Hong C-Y, Pan C-Y (2002) Chem Commun 2002(23):2800–280.1
102. Hong J, Wang Q, Fan Z (2006) Macromol Rapid Commun 27:57–62
103. Ebeling B, Eggers M, Vana P (2010) Macromolecules 43:10283–10290
104. Rossner C, Ebeling B, Vana P (2015) Design strategies for the fabrication of tailored nanocomposites via RAFT polymerization. In: Matyjaszewski K (ed) ACS symposium series. American Chemical Society, Washington, DC
105. Du B, Chen X, Zhao B, Mei A, Wang Q, Xu J, Fan Z (2010) Nanoscale 2:1684–1689
106. Hussain I, Wang Z, Cooper AI, Brust M (2006) Langmuir 22:2938–2941
107. Maye MM, Lim I-IS, Luo J, Rab Z, Rabinovich D, Liu T, Zhong C-J (2005) J Am Chem Soc 127:1519–1529
108. Rossner C, Ebeling B, Vana P (2013) ACS Macro Lett 2:1073–1076
109. Mori H, Seng DC, Zhang M, Müller AHE (2002) Langmuir 18:3682–3693
110. Dey P, Blakey I, Thurecht KJ, Fredericks PM (2013) Langmuir 29:525–533
111. Dey P, Blakey I, Thurecht KJ, Fredericks PM (2014) Langmuir 30:2249–2258
112. Dey P, Zhu S, Thurecht KJ, Fredericks PM, Blakey I (2014) J Mater Chem B 2:2827–2837
113. Rossner C, Vana P (2014) Angew Chem Int Ed 53:12639–12642
114. Ploshnik E, Langner KM, Halevi A, Ben-Lulu M, Müller AHE, Fraaije JGEM, Sevink GJA, Shenhar R (2013) Adv Funct Mater 23:4215–4226
115. Halevi A, Halivni S, Oded M, Müller AHE, Banin U, Shenhar R (2014) Macromolecules 47:3022–3032
116. Jiang W, Schalley CA (2009) Proc Natl Acad Sci USA 106:10425–10429
117. Jiang W, Schäfer A, Mohr PC, Schalley CA (2010) J Am Chem Soc 132:2309–2320